Chemical oxidation of a coordinated PNP-pincer ligand forms unexpected Re-nitroxide complexes with reversal of nitride reactivity

Gannon P. Connor, Brandon Q. Mercado, Hannah M. C. Lant, James M. Mayer, and Patrick L. Holland**

Department of Chemistry, Yale University, New Haven, Connecticut 06511, USA

ABSTRACT: Because of the thermodynamic demands of N_2 cleavage, N_2-derived nitride complexes are often unreactive. The development of multistep N_2 functionalization reactions hinges on methods for modulating nitride reactivity with supporting ligands. Here, we describe the reactions of N_2-derived Re-nitride complexes, including the first Re nitrides supported by a nitroxide-containing pincer ligand, and unusual examples of Re^{6+}-nitride complexes. The previously reported N_2-derived complex (PNP)Re(N)(Cl) (PNP = $N(CH_2CH_2P^tBu_2)_2$) can be oxidized by O-atom transfer to the backbone amide to form a novel nitroxide-pincer complex or by $1e^-$ to form a rare $S = ½$ Re^{6+}-nitride complex. The Re-nitrido interaction in a series of Re- and ligand-oxidized complexes is characterized using ^{15}N NMR spectroscopy, IR spectroscopy, and DFT calculations, and shows changes in the Re—N bond order from both ligand- and metal-centered oxidations. Chemical oxidation of the supporting ligand to form a nitroxide-pincer ligand results in subtle electronic changes at Re and a more electron-deficient nitride ligand. Combined

ligand- and metal-centered oxidation to form a Re^{6+}-nitroxide complex results in a reversal of reactivity at the nitride ligand from nucleophilic to electrophilic. These systematic electronic structure and reactivity studies demonstrate methods for inducing reactivity in N_2-derived nitride complexes.

Introduction

A growing number of systems can reductively cleave dinitrogen (N_2) to form metal nitride complexes.[1-13] In order to take advantage of these discoveries, it is now important to learn how to control the reactivity of metal-nitrido complexes. Functionalization of N_2-derived nitrides is particularly challenging because these systems tend to have strong metal-nitride bonds that are formed through thermodynamically favorable N_2 splitting. Despite this challenge, there are some examples where reductive functionalization of N_2-derived, metal-nitride complexes have been reported,[13-20] including some that feature pincer-type supporting ligands.[8-10, 21] However, in other cases, supporting ligands react preferentially to the nitride ligand.[5, 8] These disparate results highlight the difficulty of predicting the reactivity of N_2-derived metal-nitrido complexes and show the need for understanding how nitrides respond to the supporting ligand. Understanding how supporting ligands control reactivity at the nitride ligand of these complexes is therefore key to developing systems that can achieve both the difficult reductive cleavage of N_2 as well as subsequent functionalization of the nitride ligand to useful products. In addition, chemists need to contend with the selectivity of attack on the supporting ligand versus attack on the nitride, as described below.

Metal-bound nitrides are known to range from strongly nucleophilic to strongly electrophilic,[22-24] including some complexes in which the nitride ligand can react in an ambiphilic fashion.[25] Here, we study the reactivity of (PNP)Re(N)(Cl) (**1**, PNP = $N(CH_2CH_2P^tBu_2)_2$), which forms from the reductive cleavage of N_2 by $(PNP)ReCl_2$.[8, 11] Schneider has reported that complex **1** reacts with H^+ at the supporting ligand to protonate the backbone amide but reacts with carbon electrophiles at the nitride ligand to form alkylimido complexes, suggesting a fine balance between nitride and supporting ligand reactivity.[8, 21] We thus were interested to explore other electrophiles in efforts toward net N_2 functionalization to other products.

The $Re^{6+/5+}$ potential in tetrahydrofuran (THF) for **1** is –0.08 V vs. $Cp_2Fe^{+/0}$,[8] which suggests that its formally Re^{5+} center is surprisingly electron-rich. We reasoned that **1** could display reactions toward O-atom donors that would form new N–O bonds to the N_2-derived nitride, giving interesting functionalized products such as nitrosyl or nitro complexes. The transformation of electrophilic nitride ligands to nitrosyl ligands has been reported in metal-nitrido complexes[26-30] and oxidation of nitrosyl to nitro ligands is also well precedented,[31-35] but neither has been observed in nitrides derived from N_2. To assess these possibilities, as well as to explore new methods to quantify and modulate the reactivity of metal-nitrido complexes, we experimentally evaluated the oxidative reactivity of **1** with O-atom transfer reagents and $1e^-$ chemical oxidants. These studies not only serve to help expand the understanding of supporting-ligand versus nitride-ligand reactivity in systems that can cleave N_2, but could also address new pathways of transition-metal-mediated N_2 functionalization.

Results and Discussion

Synthesis and characterization of a novel nitroxide-pincer complex. Complex **1** reacts with 1.5 equiv of 3-chloroperbenzoic acid (mCPBA) to give a new diamagnetic complex **2** at ambient temperature in THF or diethyl ether (Et_2O). This reaction proceeds in >95% yield when monitored by ^1H and $^{31}P\{^1H\}$ NMR spectroscopy. The oxidation of **1** to **2** leads to a slight shift in the ^{31}P resonance of the phosphine arms from δ 84.6 ppm for **1** to δ 64.6 ppm for **2** in the $^{31}P\{^1H\}$ NMR spectrum collected in THF-d_8. The solid-state crystal structure of **2** reveals that the oxidation occurs at the backbone amide of the pincer ligand rather than at the nitride ligand, forming a nitroxide moiety that binds η^2 to the metal center (Scheme 1). In the crystallographic structure of **2**, the nitroxide O atom has a hydrogen-bond to a molecule of 3-chlorobenzoic acid (mCBA) in the solid state (see Fig. S39), and **2** is isolated with one equivalent of mCBA as evident from the ^1H NMR spectrum of crystals of **2** (see Fig. S1). The H-atom involved in the hydrogen-bond was not resolved by X-ray crystallography, but DFT calculations, structural parameters, and reduction potentials all suggest that the mCBA molecule is protonated rather than the Re-bound nitroxide (see below). Reaction of **1** with 1.5 equiv H_2O_2 (as a 30% w/w solution in H_2O) also forms **2** in 23% yield according to $^{31}P\{^1H\}$ NMR spectroscopy in THF-d_8 (see Fig. S5). Due to the low spectroscopic yield, we did not attempt to isolate **2** from the reaction of **1** with H_2O_2. Additionally, attempts to isolate **2** without a hydrogen-bonded mCBA equivalent were not successful. Although numerous transition metal complexes with nitroxide or hydroxylamine ligands have been reported,[36-38] only one other example of forming a nitroxide ligand via oxidation of a coordinated amide ligand has been reported with any transition metal.[39] No examples of a nitroxide coordinated

to Re have been reported to our knowledge. Thus, this reaction represents a distinctive example of chemical oxidation of a coordinated pincer ligand to form a nitroxide ligand.

In contrast, **2** is not formed when nucleophilic O-atom transfer reagents are employed. For example, reaction of **1** with excess trimethylamine-*N*-oxide, pyridine-*N*-oxide, or iodosobenzene gave no conversion to **2** by ^{1}H and ^{31}P{^{1}H} NMR spectroscopies, even after prolonged heating at 115 °C. Instead, these reactions gave an intractable mixture of multiple products, if any (see Fig. S6-8). IR spectra of the crude reaction products show no evidence of nitrosyl formation. These results suggest that oxidized products of these reactions involve neither O-atom transfer to the amide backbone nor the nitride ligand. The reactivity of **1** with an oxygen electrophile (mCPBA) at the backbone amide to form **2** differs from the reactivity of **1** with carbon electrophiles, which react at the nitride ligand to form a new N–C bond.[8, 21] However, formation of **2** in this reaction is more reminiscent of ligand-based reactivity of **1** with hydrochloric or triflic acid (HOTf) to form cationic complexes with the amide protonated (Scheme 1).[8]

Scheme 1. Oxidative reactivity of Re-nitride complex **1** and formation of novel nitroxide complexes **2** and **4**.

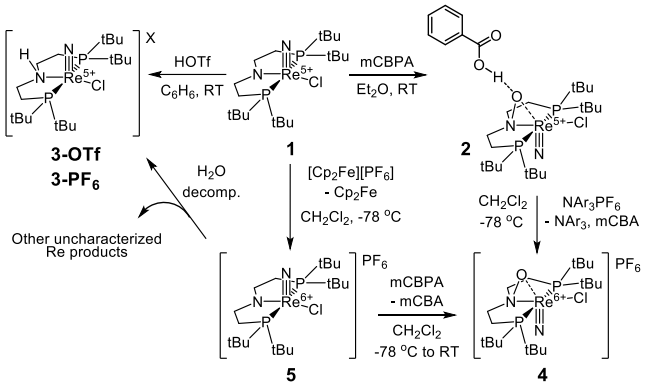

While the amide backbones in PNP-pincer ligands[40-48] are strong σ- and π-donors, it is not obvious how to view the bonding nature of the new "$P^{O}NP$"-pincer ligand that features a nitroxide backbone. The solid-state structure of **2** exhibits a long Re–O interaction of 2.306(6) Å, and the Re-amide bond length elongates slightly from 2.033(6) to 2.080(7) Å going from **1** to **2**, respectively (Fig. 1). There is also a slight shortening of the Re–Cl bond length from 2.441(2) Å to 2.409(2) Å upon oxidation of the supporting ligand, which is consistent with a loss of electron density at the metal center. Otherwise, the coordination geometry around Re deviates little from **1** to **2** (Fig. 2a). To explore the change in electron density at Re, cyclic voltammetry (CV) experiments on **1** and **2** were performed in THF. These experiments show an anodic shift of the $Re^{6+/5+}$ couple of 80 mV from –0.08 V vs. $Cp_2Fe^{+/0}$ for **1** to 0.00 V vs. $Cp_2Fe^{+/0}$ for **2** (Fig. 3).[8] This represents quite a small shift in electron-richness between **1** and **2** despite chemical oxidation of the supporting ligand. This observation agrees with the lack of change in the coordination geometry around Re. For comparison, protonation of **1** with HOTf to form the cationic amide-protonated complex [($P^{H}NP$)Re(N)(Cl)][OTf] (**3-OTf**) has a much larger effect, shifting the Re^{5+} to Re^{6+} reduction potential to 0.60 V vs. $Cp_2Fe^{+/0}$. These data show that there are only subtle electronic changes between **1** and **2**, supporting the conclusion that the ligand in **2** is a nitroxide anion with a hydrogen bonded carboxylic acid, rather than a hydroxylamine ligand. The small changes between **1** and **2** indicate that oxidation of the amide of a PNP-pincer complex to a nitroxide may offer an opportunity to "fine-tune" the electronics of the complex to improve reactivity without changing its overall charge or requiring the synthesis of a separate ligand.

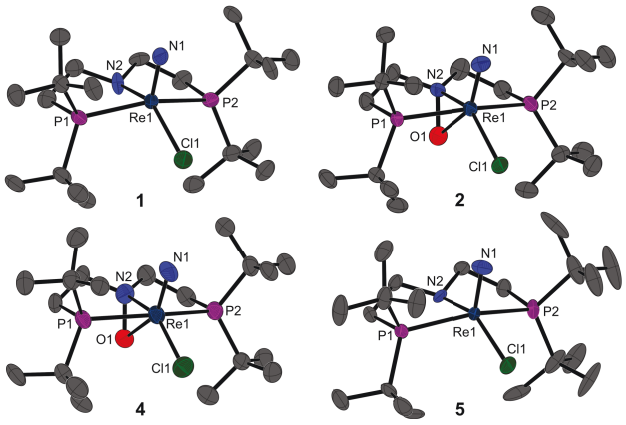

Figure 1. Solid-state structures of parent nitride complex **1** (left, matches previously reported DFT structure[8]), Re^{5+}-nitroxide complex **2** (mCBA molecule omitted), Re^{6+}-nitroxide complex **4** (PF_6 ion omitted), and Re^{6+}-nitride complex **5** (PF_6 ion omitted) with thermal ellipsoids at 50% probability. Hydrogen atoms are omitted for clarity.

Table 1 Selected bond lengths (Å) and bond angles (°) of complexes **1**, **2**, **4**, and **5**.

Bond/Angle	**1**	**2**	**4**	**5**
Re1–N1	1.643(6)	1.638(7)	1.665(7)	1.650(5)
Re1–N2	2.033(6)	2.080(7)	2.097(8)	2.054(5)
Re1–Cl1	2.441(2)	2.409(2)	2.295(3)	2.339(2)
Re1–O1	-	2.306(6)	2.200(6)	-
Re1–P1	2.443(2)	2.443(2)	2.516(2)	2.476(2)
Re1–P2	2.435(2)	2.460(2)	2.507(2)	2.479(2)
O1–N2	-	1.436(9)	1.433(1)	-
N1–Re1–N2	105.8(3)	105.3(3)	105.0(4)	103.4(2)
N1–Re1–Cl1	106.5(2)	105.3(2)	103.1(3)	105.6(2)
N2–Re1–Cl1	147.7(2)	149.5(2)	151.9(2)	151.0(1)
N1–Re1–P1	100.4(2)	96.1(3)	95.8(3)	98.9(2)
N1–Re1–P2	99.9(2)	97.6(3)	96.5(3)	100.8(2)
O1–N2–Re1	-	79.7(4)	74.5(4)	-
O1–Re1–N2	-	37.8(2)	38.8(3)	-
O1–Re1–Cl1	-	111.7(2)	113.1(2)	-

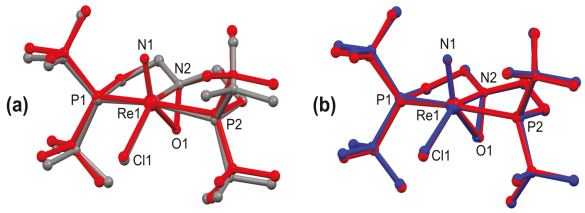

Figure 2. (a) Overlay of solid-state structures for Re^{5+}-nitride (**1**, gray), and Re^{5+}-nitroxide (**2**, red). **(b)** Overlay of solid-state structures for Re^{5+}-nitroxide (**2**, red) and Re^{6+}-nitroxide (**4**, blue).

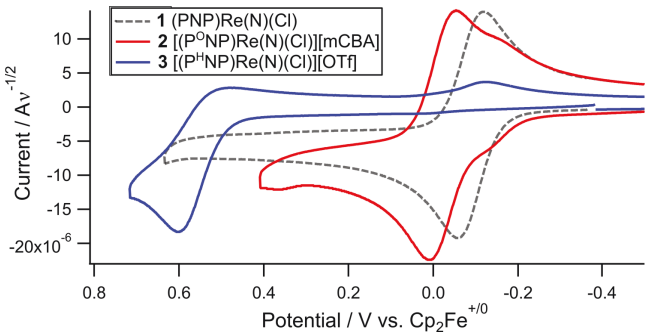

Figure 3. Cyclic voltammograms of **1** (gray, dashed), **2** (red), and **3-OTf** (blue) demonstrating effect of functionalizing the backbone amide on the $Re^{6+/5+}$ redox potential. Details: 100 mV/s scan rate, scanning anodically in 0.1 M tetrabutylammonium hexafluorophosphate solution in THF with glassy carbon disk working, Pt wire auxiliary, and Ag wire psuedoreference electrodes. An additional redox feature in the voltammogram of **2** may be from a minor adventitious impurity.

In order to elucidate the changes in bonding interactions arising from formation of the nitroxide, complexes **1** and **2** were modelled using DFT calculations. Complex **2** was modelled with and without a coordinated mCBA molecule, and the presence of mCBA did not significantly affect any of the computational results (see SI). Natural bond order (NBO) analysis of **2** (without mCBA) identifies a weak Re–O interaction with a Wiberg bond order[49] of 0.22, which is consistent with the long Re–O bond observed in the solid-state structure (Fig. 4). The

Wiberg bond order of the Re-amide decreases from 0.65 in **1** to 0.43 in **2**, suggesting loss of π-donation from the amide. Second-order perturbation theory (SOPT) analysis[50] identifies several donor-acceptor interactions between the nitroxide and Re-containing molecular orbitals. This analysis estimates the energy lowering in a molecule achieved by donation of electrons in a filled (bonding or lone pair) orbital into a vacant or antibonding orbital. The dominant interaction identified by SOPT analysis is the donation of lone pairs (LPs) on the O atom into antibonding *d*-π* Re-nitride orbitals (Fig. 4c). These interactions replace analogous donation from the amide LP in **1** into the same antibonding *d*-π* Re-nitride orbitals. However, the donor-acceptor interactions from the O atom in **2** are stronger than the analogous interactions from the amide in **1**, as evident by an approximately 30% increase in the calculated exchange energies for these interactions in **2** vs. **1** (see SI for more details). Additionally, a weak donor-acceptor interaction between the N–O σ-bond and the overlapping antibonding Re-nitride orbital was identified in **2**.

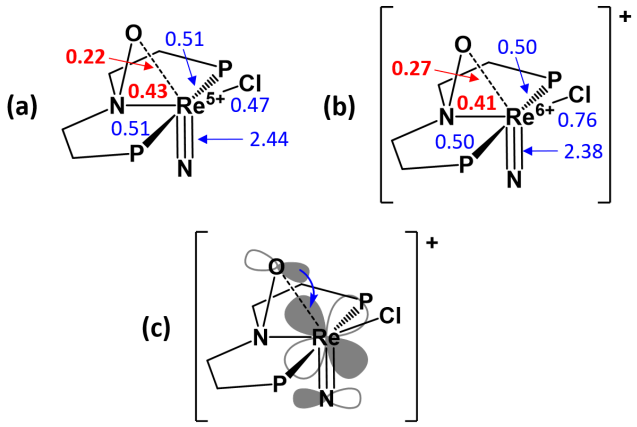

Figure 4. Calculated Wiberg bond orders of **(a)** Re^{5+}-nitroxide complex (**2**) and **(b)** Re^{6+}-nitroxide complex (**4**), and **(c)** representation of donor-acceptor interaction from O atom LP to antibonding *d*-π* Re-nitride orbital. For the purpose of clarity, the supporting ligand is truncated.

Overall, the change from **1** to **2** decreases the reactivity of the complex. Nitroxide complex **2** does not react with mCPBA, trimethylamine-*N*-oxide, pyridine-*N*-oxide, or iodosobenzene. In addition, **2** does not react with potential nucleophiles PMe_3 or PPh_3. Thus, it is apparent that introduction of the nitroxide moiety does not affect the strong Re-nitrido interaction enough to increase reactivity at the nitride ligand.

Synthesis of Re^{6+}-nitride complexes. The reversible anodic waves observed in CV experiments of **2** indicate that the $(P^{O}NP)Re^{6+}$ complex could be accessible. Oxidation of **2** at –78 °C in dry CH_2Cl_2 with tris(4-bromo-phenyl)aminium hexafluorophosphate affords $[(P^{O}NP)Re(N)(Cl)][PF_6]$ (**4**), a rare example of an isolable paramagnetic Re^{6+}-nitride species. Complex **4** shows several broad paramagnetic proton resonances in its ^1H NMR spectrum between δ 5.5 and δ 34.0 ppm in CD_2Cl_2 (see Fig. S2), and its EPR spectrum is reminiscent of the few other reported $S = ½$ Re^{6+}-nitride complexes (see Fig. S12).[51-53] The solid-state structure of **4** shows a shortening of the Re–O interaction by 0.1 Å to 2.200(6) Å (Fig. 2b). The Re-nitride and Re-amide bond distances remain similar between **2** and **4**, but the Re–Cl bond distance shortens by about 0.1 Å from 2.409(2) to 2.295(3) Å upon oxidation of the Re metal center. NBO analysis of the DFT model of **4** calculates a larger Wiberg bond order of 0.27 for the Re–O bond and diminished value of 0.41 for the Re-amide bond in agreement with the shortening of the Re–O bond and slight lengthening of the Re-amide bond, respectively (Fig. 4). SOPT analysis identifies the same donor-acceptor interactions in **4** as in **2**; however, oxidation of the metal center in **4** results in a 60%

increase in exchange energies of the donation from O atom LPs into the antibonding *d*-π^* Re-nitride orbitals.

CV analysis of parent nitride **1** shows a reversible $Re^{6+/5+}$ couple in dry CH_2Cl_2,[8] suggesting that the PNP-Re^{6+} species is accessible in this case as well. This redox event becomes less reversible in dry acetonitrile and is only quasi-reversible in dry THF, becoming more irreversible with added aliquots of H_2O, indicating the instability of the Re^{6+} oxidation product (see Fig. S11). Oxidizing **1** in dry CH_2Cl_2 at –78 °C with $[Cp_2Fe][PF_6]$ results in a color change from orange to red, and the 1e^- oxidized complex $[(PNP)Re(N)(Cl)][PF_6]$ (**5**) was isolated from the reaction as a crystalline solid in 76% yield. EPR spectroscopy of the isolated crystals provides a spectrum similar to that of **4** (see Fig. S13).[51-53] However, ^1H and $^{31}P\{^1H\}$ NMR spectroscopies indicate that the crystals contain approximately 25% of a diamagnetic impurity, identified as $[(P^{H}NP)Re(N)(Cl)][PF_6]$ (**3-PF$_6$**), where $P^{H}NP$ indicates the pincer ligand with protonated nitrogen. Upon further investigation, **5** was found to be extremely sensitive to decomposition in the presence of traces of moisture, forming **3-PF$_6$** as the major product (see Fig. S4, S11). Complex **3-PF$_6$** is structurally and spectroscopically analogous to the related triflate salt **3-OTf** (see Fig. S4, S43).[8]

Characterizing Re-nitrido interactions via ^{15}N-isotope labelling. With this series of Re-nitride complexes oxidized at the supporting ligand and/or metal center, we sought to quantitatively study the effects of these oxidations on the Re-nitrido bond via isotope labelling experiments. The ^{15}N-labeled parent nitride (**1-^{15}N**) was synthesized from reaction of $(PNP)ReCl_2$ with terminally labeled $[PPN][N{=}N{=}^{15}N]$,[8] resulting in 50% labelling of the nitride ligand with ^{15}N. The 50% ^{15}N-labeled nitride complexes **2-^{15}N**, **3-^{15}N**,[8] **4-^{15}N**, and **5-^{15}N** were subsequently prepared from **1-^{15}N**.

Isotopic labelling of the nitride ligand enables direct spectroscopic comparison of the Re-nitride stretching frequencies in the IR spectra of these complexes, and the ^{15}N resonance for the nitride is easily observed in the ^{15}N NMR spectra of the diamagnetic Re^{5+} complexes **1-^{15}N**, **2-^{15}N**, and **3-^{15}N**. Additionally, the Re-nitride bond lengths are available from the solid-state structures of the complexes. The data in Table 2 show that Re-nitride interaction varies throughout the series of complexes, demonstrating small changes in Re-nitride bond lengths and notable changes in Re-nitride stretching frequencies. For example, the Re-nitride stretching frequency ranges from 1024 cm^{-1} in **4-^{15}N** to 1075 cm^{-1} in **3-^{15}N**, a difference of 51 cm^{-1}. In general, we see that functionalization of the backbone amide results in slightly higher Re-nitride stretching frequencies, while oxidation of the metal center results in slightly lower frequencies. However, the Re-nitride bond length ranges only from 1.624(7) Å in **3-OTf** to 1.665(7) Å in **4**. Excluding the protonated complex **3-OTf**, the complexes adhere well to Badger's rule, which predicts a correlation between bond length and stretching frequency (Fig. 5a).[54] It is worth noting that the backbone- *and* metal-oxidized complex **4-^{15}N** demonstrates the lowest Re-nitride stretching frequency, likely resulting from stronger donation from O atom LPs into the antibonding *d-π** Re-nitride orbitals. Assuming that changes in stretching frequency parallel changes in bond strength, this implies that **4-^{15}N** has the weakest Re-nitride interaction.

The chemical shifts of the ^{15}N nitride resonances in the ^{15}N NMR spectra of **1-^{15}N**, **2-^{15}N**, and **3-^{15}N** suggest the *relative* electron density of the nitride ligands, at least to a first approximation. In organic compounds, ^{15}N NMR chemical shifts have been shown to be correlated to various chemical properties, including Lewis basicity.[55-59] We wondered whether the ^{15}N NMR chemical shifts of the nitride ligands could thus be an estimate of the relative electron richness of these ligands and, by extension, be used to predict reactivity.

Functionalization of the amide in **1-**^{15}**N** to form a nitroxide (**2-**^{15}**N**) or protonated amide (**3-**^{15}**N**) both shift the nitride ^{15}N resonance downfield, suggesting a decrease in Lewis basicity. This can be rationalized partially from first principles, since oxidation or protonation of the complex should give a more electron-deficient Re center, which in turn should facilitate stronger donation from the nitride ligand. However, the changes in the nitride ^{15}N chemical shift from **1-**^{15}**N** to **2-**^{15}**N** (22 ppm) and from **1-**^{15}**N** to **3-**^{15}**N** (16 ppm) are very close. Despite the similar ^{15}N-nitride chemical shifts, there is a significant change in $Re^{6+/5+}$ reduction potential of +520 mV for **3** vs. **2**. Indeed, **2**, which has a more electron-*rich* Re center than **3** based on their relative Re^{6+} reduction potentials, is predicted to have the most electron-*deficient* nitride by ^{15}N NMR spectroscopy, assuming that the chemical shifts show the same correlations with electron density in **1**–**3** as in organic compounds. This suggests that the electron-richness of the Re center may not be the only factor affecting the electron-richness of the nitride ligand. However, it is worth noting that difference in charge between **3** and **1**-**2** may also play a large role in the differences in redox potentials between the complexes; furthermore, since **1**–**3** are generally unreactive at the nitride, we could not experimentally test the Lewis basicity trends hinted by the ^{15}N NMR chemical shifts.

Table 2 Re–^{15}N stretching frequencies, bond lengths, and ^{15}N NMR chemical shifts for Re-nitrido complexes

Complex	Re–^{15}N stretch (cm^{-1})	Re–N bond length (Å)	Nitride ^{15}N NMR chemical shift[a] (ppm)
(PNP)Re(N)(Cl) (**1-**^{15}**N**)	1037	1.643(6)	371
[(P^{O}NP)Re(N)(Cl)][mCBA] (**2-**^{15}**N**)	1042	1.638(7)	393

[(P^{H}NP)Re(N)(Cl)][OTf] (**3-**^{15}**N**)	1075	1.624(7)[b]	387
[(P^{O}NP)Re(N)(Cl)][PF_6] (**4-**^{15}**N**)	1024	1.665(7)	-
[(PNP)Re(N)(Cl)][PF_6] (**5-**^{15}**N**)	1035	1.650(5)	-

[a] Chemical shift reported vs. CH_3NO_2. [b]This distance has been previously reported as 1.659(2) Å.[3] We remeasured this distance as 1.624(7) Å from a crystal with a different unit cell, and the shorter bond distance more closely corresponds to the high Re–N stretching frequency in this complex as well as its higher calculated Re–N Wiberg bond order.

To supplement our spectroscopic studies, we compared the DFT models of complexes **1–5**. These models demonstrate that oxidation of the amide to form a nitroxide has an effect on the distribution and relative energy of the frontier molecular orbitals. The perturbation of molecular orbitals by replacing Re-amide interactions with Re-nitroxide interactions may be responsible for the decreased electron-richness of the nitride ligand in complex **2** vs. complex **3**. The redox trends between **1**, **2**, and **3** are reproduced with DFT calculations using these models, which validates the accuracy of the computational method (see SI). NBO analysis of the series predicts changes in the Re-nitride Wiberg bond orders that match the experimentally observed trends in Re-nitride stretching frequencies (Fig. 5b and 6). These trends indicate that oxidation of the Re metal center results in a slight decrease in Re-nitride partial bond order, with **4** having the lowest Re-nitride bond order of 2.38.

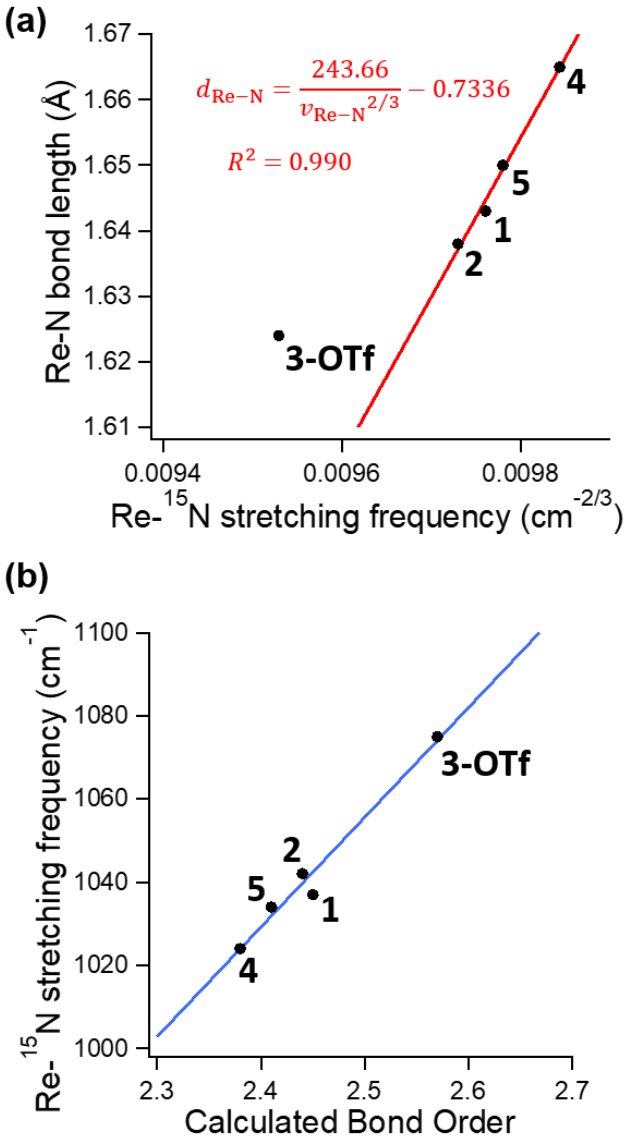

Figure 5. Re-nitride bond length vs. $1/\nu_{Re-N}^{2/3}$, with Badger's rule demonstrated as a linear fit for complexes **1**, **2**, **4**, and **5**. **(b)** Calculated Wiberg bond order of Re-nitride bonds vs. observed Re-nitride stretching frequencies in complexes **1**–**5**.

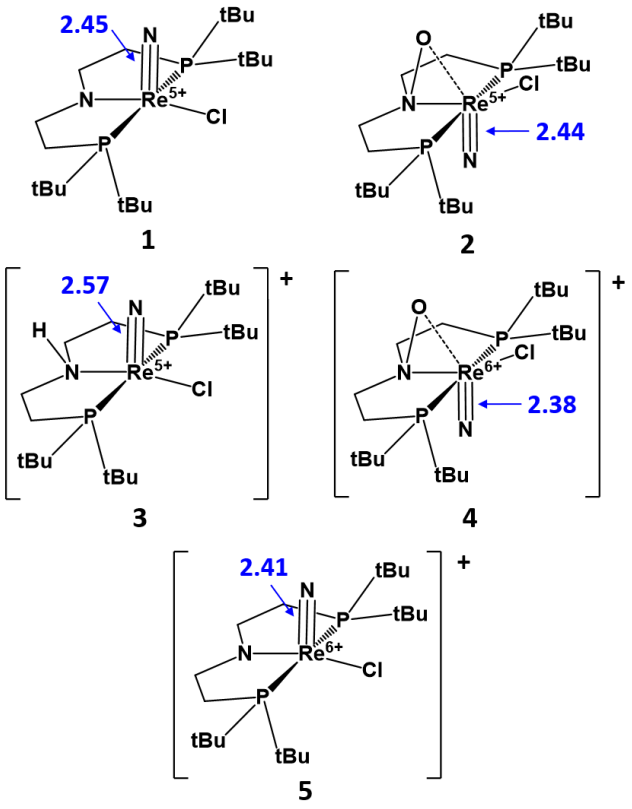

Figure 6. Calculated Wiberg bond order of Re-nitride bonds in complexes **1**–**5**.

Oxidation-induced change in nitride reactivity. At ambient temperature in CD_2Cl_2, addition of 1.2 equiv of PPh_3 to **4** leads to slow formation over the course of several hours of a new product (Scheme 2, drawn as **6**). The $^{31}P\{^1H\}$ NMR spectrum of the solution shows two singlets in a 2:1 ratio at δ 71.6 ppm and δ 54.6 ppm, respectively. Formation of this product is accompanied by loss of the PPh_3 signal, which is matched by an analogous change in the PPh_3 resonances in the corresponding ^1H NMR spectra. These data are consistent with formation of a diamagnetic Re^{3+}-phosphinimide complex, which would require an additional $1e^-$ reduction of the complex formed from initial $2e^-$ reduction of the nitride to phosphinimide. To determine whether **6** is indeed a phosphinimide complex, PPh_3 was reacted with **4**-^{15}**N**. This resulted in splitting of

the ^{31}P resonance at δ 54.6 ppm into a doublet (J = 35.1 Hz), demonstrating that PPh_3 binds to the ^{15}N-labeled nitride (Fig. 7, inset).

Scheme 2. Formation of phosphinimide complex **6** upon addition of PPh_3 to **4**.

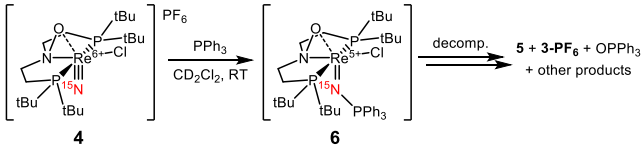

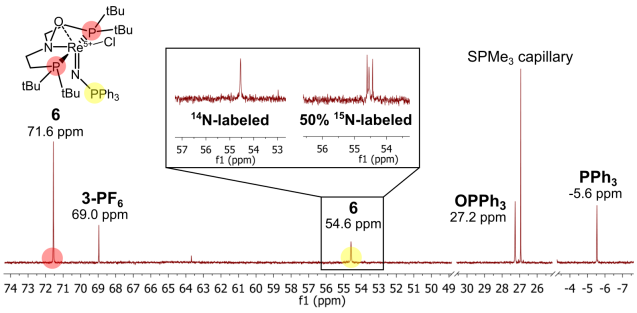

Figure 7. ^{31}P{^{1}H} NMR spectrum of **4** with PPh_3 in CD_2Cl_2 after 15 hours showing formation of a phosphinimide intermediate **6**. **Inset:** Difference in splitting of ^{31}P resonance at δ 54.6 ppm depending on N isotope used.

Formation of a phosphinimide from **4** with phosphines can involve the nitride acting either as an electrophile[24] or, less commonly, a nucleophile.[60] To assess the nature of the transition state during the reaction of the nitride ligand in **4** with phosphines, we varied the phosphines with substituents of differing electron richness. When **4** is mixed with stoichiometric tris-(*p*-tolyl)phosphine (P(*p*-tolyl)$_3$) or tris-(4-fluorophenyl)phosphine (P(4-^{F}Ph)$_3$), formation of phosphinimide complexes **6-P(*p*-tolyl)$_3$** and **6-(4-^{F}Ph)$_3$**, respectively, is observed by ^{1}H and ^{31}P{^{1}H} NMR spectroscopy (Fig. S22-S25). Since ^{1}H and ^{31}P{^{1}H} NMR spectra indicate that the phosphinimide complex is the first product observed from reaction of **4** with phosphines,

following the disappearance of the distinct UV-Vis absorbance feature of **4** with λ_{max} = 668 nm allowed us to qualitatively compare the rates of phosphinimide complex formation. To determine the kinetic preference of **4** for phosphines of different electron-richness, we compared the consumption of **4** in the presence of P(4-^{F}Ph)$_3$, PPh$_3$, and P(*p*-tolyl)$_3$ under pseudo-first order conditions (10 equiv phosphine). Under identical reaction conditions, **4** reacts more quickly in the presence of P(*p*-tolyl)$_3$ than PPh$_3$, which in turn reacts more quickly than P(4-^{F}Ph)$_3$ (Fig. S26). Since consumption of **4** corresponds to formation of the phosphinimide complex **6**, the rate of P–N bond formation is more rapid for more nucleophilic phosphines. This observation indicates that the nitride ligand in **4** behaves as an electrophile. Furthermore, in a competition experiment containing 1 equiv of both P(*p*-tolyl)$_3$ and P(4-^{F}Ph)$_3$, **4** reacts preferentially with P(*p*-tolyl)$_3$ to form **6-P(*p*-tolyl)$_3$** (Scheme 3), and no formation of **6-P(4-^{F}Ph)$_3$** is observed (Fig. S27-S28). The addition of excess P(*p*-tolyl)$_3$ to solution containing **6-P(4-^{F}Ph)$_3$** results in conversion of the phosphinimide complex to **6-P(*p*-tolyl)$_3$** within 10 minutes, suggesting a labile N–P interaction that favors the more electron-rich phosphinimide (Fig. S29). This is evidence of a thermodynamic preference for formation of the more electron-rich phosphinimide due to a stronger N–P interaction.

Scheme 3. Competition reaction between P(*p*-tolyl)$_3$ and P(4-^{F}Ph)$_3$ with **4**.

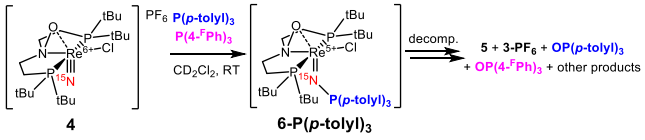

It is significant that only complex **4**, in which both the backbone amide and metal center of **1** have been oxidized, was found to react with phosphines to form transiently observed phosphinimide products. This demonstrates that the nitride in **4** is electrophilic enough to

undergo reaction with nucleophiles, representing a reversal of reactivity at the nitride ligand relative to **1**, wherein the nitride reacts as a nucleophile with carbon electrophiles.[8, 21] Importantly, *umpolung* that makes the nitride electrophilic appears to require *both* oxidation of the backbone to form a nitroxide *and* 1e^- oxidation of the metal center to form a Re^{6+} complex, as neither **2** (just oxidized at ligand) nor **5** (just oxidized at Re) react with phosphine nucleophiles (Fig. S30-31). Since **2** and **5** do not react with phosphines, it suggests that neither 1e^- reduction of **4** (to form **2**) nor O-atom abstraction from the nitroxide in **4** (to form **5**) occurs prior to phosphinimide formation.

The phosphinimide product **6** is unstable under the reaction conditions and decomposes to **3-PF**$_6$ (^{31}P resonance at δ 69 ppm), a paramagnetic complex (which resembles **5** by ^{1}H NMR spectroscopy), and $OPPh_3$, among other unidentified phosphorus-containing products. The concentration of **6** during the reaction reached a maximum 15 hours into the reaction at approx. 31% spectroscopic yield by integration vs. an internal standard under these conditions (Fig. 7). The instability of **6** has precluded its isolation as a pure material. The formation of **3-PF**$_6$, the paramagnetic species, and $OPPh_3$ is observed only after **6** is formed, which suggests that $OPPh_3$ is formed by net O-atom abstraction from the nitroxide to a PPh_3 (see SI). This could either be from the phosphinimide or free PPh_3 in the reaction. However, in phosphinimide-forming reactions that contain both P(*p*-tolyl)$_3$ and P(4-^{F}Ph)$_3$, phosphine oxides of both phosphines are observed as decomposition products (see Fig. S28). The observation of OP(4-^{F}Ph)$_3$ indicates that one mechanism of decomposition is likely the abstraction of the nitroxide O-atom by free phosphine in solution, since **6-P(4-^{F}Ph)**$_3$ is not observed under these conditions.

DFT analysis of the atomic contributions to the lowest-unoccupied molecular orbitals (LUMOs) of **1–5** provides a rationalization for this reversal in reactivity (see Tables S15-19). In complex **4**, the LUMO and LUMO+1 are more localized at the nitride ligand than in the rest of the series, which is consistent with increased electrophilic behavior at the nitride (Fig. 8). Thus, the cooperative effect of ligand-centered and metal-centered oxidations has a notable effect on nitride reactivity despite the strong Re-nitrido interaction.

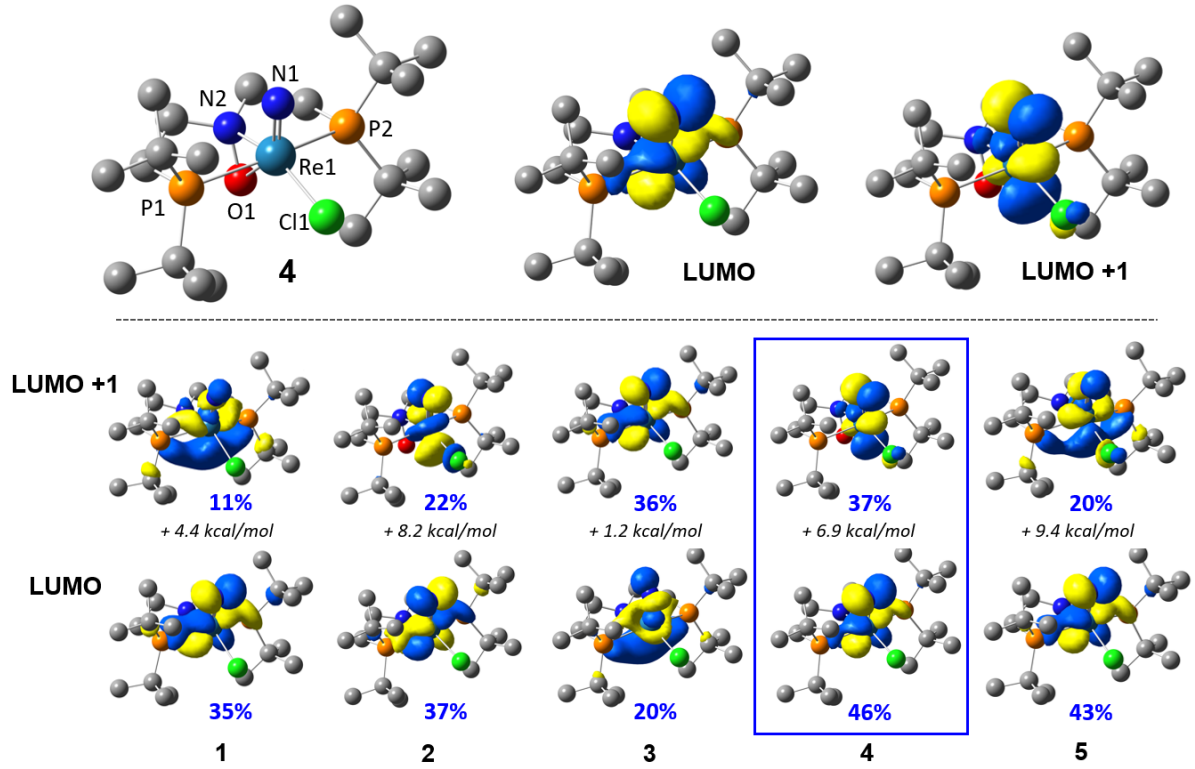

Figure 8. Top: DFT model of complex **4** and visualizations of LUMO and LUMO+1 molecular orbitals (isosurface value = 0.05). **Bottom:** Drawings of the LUMO and LUMO+1 orbitals for **1–5** with atomic contributions of the nitride (blue percentages) showing that **4** demonstrates the highest combined nitride contribution to the lowest unoccupied frontier orbitals (energy difference between molecular orbitals denoted in italics).

Conclusions

This work describes the oxidative reactivity of an N_2-derived metal-nitrido complex, wherein two kinds of oxidations have been observed. Outer-sphere agents oxidize the metal center, forming unusual Re^{6+}-nitrido complexes. Electrophilic O-atom transfer agents, however, transfer O to the amide portion of the pincer ligand to form a nitroxide. Cooperative changes in oxidation state and ligand oxidation are required to induce electrophilic reactivity in the normally unreactive nitride complex. Our studies also uncover the unusual formation of Re complexes supported by nitroxide-containing pincer ligands that provide a new variant on a well-characterized PNP pincer. The O-atom transfer to the supporting ligand suggests that careful consideration of the supporting ligand is required for conversion of N_2 to oxidized N species.

Formation of the nitroxide moiety causes electronic changes at the metal center by replacing amide LP interactions with O atom LP interactions, resulting in a redistribution of molecular orbitals. These changes have a surprisingly small effect on the strong Re-nitride interaction in these complexes, but, when coupled with $1e^-$ oxidation of the metal center, cause the nitride ligand to become electrophilic. This *umpolung* in reactivity at the nitride ligand is achieved without exchanging any of the supporting ligands, potentially offering a new strategy for "fine-tuning" metal-center electronics via oxidation of a supporting amide ligand to a nitroxide.

Experimental Section

General considerations. All manipulations were performed under an inert atmosphere of N_2 gas in a M. Braun glovebox or on a Schlenk line unless otherwise specified. Tetrahydrofuran

(THF) was distilled under argon from potassium benzophenone ketyl and stored over molecular sieves prior to use. Unless otherwise noted, all other solvents were dried via passage through Q5 columns from Glass Contour Co. and stored over molecular sieves prior to use. Deuterated solvents were degassed and dried over calcium hydride before storing over molecular sieves prior to use, and THF-d_8 was dried additionally with potassium benzophenone ketyl. Ammonium perrhenate (Strem, 99+%), bis-[2-(di-tertbutylphosphino)ethyl)]amine (Strem, 10% w/w in hexanes), hydrogen peroxide (Fisher Chemicals, 30% in H_2O), trimethylamine-*N*-oxide (Sigma-Aldrich, 98%), pyridine-*N*-oxide (Sigma-Aldrich, 95%), iodosobenzene (TCI, 95+%), ferrocenium hexafluorophosphate (Santa Cruz Biotechnology, 97%), nitrosonium hexafluorophosphate (Alfa Aesar, 96%), tris-(4-bromophenyl)amine (Sigma-Aldrich, 98%), bis(triphenylphosphine)iminium chloride (Strem, 97%), sodium azide (terminal ^{15}N-labeled, Cambridge Isotope Laboratories, 98+%), trifluoromethanesulfonic acid (Sigma-Aldrich, 99+%), and trimethylphosphine (Sigma-Aldrich, 1.0 M in THF) were purchased and used without further purification. Triethylamine (Sigma-Aldrich, 99+%, distilled), triphenylphosphine (Aldrich, 99%, sublimed), tris(*p*-tolyl)phosphine (Aldrich, 98%, dried under high vacuum), tris(4-fluoro-phenyl)phosphine (Strem, 99%, dried under high vacuum), ferrocene (Aldrich, 98%, recrystallized), tetrabutylammonium hexafluorophosphate (Sigma-Aldrich, 99%, recrystallized x3), and *m*-chloroperbenzoic acid (Aldrich, <77%, washed with pH 8.0 buffer and extracted with Et_2O) were purified prior to use. $ReOCl_3(PPh_3)_2$,[61] $(ReCl_3(MeCN)(PPh_3)_2$,[62] $(PNP)ReCl_2$,[8] and bis(triphenylphosphine)iminium azide[63] were synthesized and purified according to literature procedures.

Syntheses. *^{15}N-labelled bis(triphenylphosphine)iminium azide:* Following a literature procedure,[64] 200 mg Na(N=N=^{15}N) (3.03×10^{-3} mol, 1 equiv) and 1.74 g (PPN)Cl (3.03×10^{-3} mol, 1 equiv) were dissolved in 50 mL EtOH and stirred at ambient temperature for 6 h. The

resulting mixture was filtered to remove NaCl, and the precipitate was washed with 15 mL EtOH. The filtrate was concentrated to dryness under vacuum to give a white solid. The residue was triturated with 3 x 10 mL Et_2O to give a white powder, which was dried in the vacuum oven at 120 °C for 24 h. *NOTE: Azide salts can be explosive. Use extreme caution and allow the azide to cool to ambient temperature before handling after or during drying*. Isolated 1.56 g fine white powder (88% yield). IR stretches matched reported values.[64]

*(PNP)Re(N)(Cl) (**1**):* Compound **1** was synthesized using a modified literature procedure.[8] Crystals suitable for X-ray diffraction were grown from a concentrated solution of **1** in pentane. ^1H and $^{31}P\{^1H\}$ NMR spectra matched previously reported data. FTIR (solid, cm^{-1}): 2983, 2942, 2922, 2897, 2861, 2814, 1467, 1390, 1368, 1326, 1281 (w), 1261 (w), 1213, 1180, 1161, 1092, 1083, 1056, 1020, 966, 939, 918, 874 (w), 809 (s), 116, 102, 612, 584, 544, 503, 478 (s), 424.

*(PNP)Re(^{15}N)(Cl) (**1-^{15}N**):* This compound was synthesized analogous to **1** via a modified literature procedure,[8] in which 20.0 mg (PNP)$ReCl_2$ (3.24×10^{-5} mol, 1.0 equiv) dissolved in 5 mL THF was added to 20.2 mg (PPN)(N=N=^{15}N) (3.47×10^{-5} mol, 1.07 equiv) slurried in 5 mL THF at –40 °C. The reaction was allowed to warm to ambient temperature and stirred for 12 h, accompanied by a color change from purple to orange and formation of a white precipitate. The solvent was removed under vacuum, and the product was extracted with 2 x 5 mL Et_2O and filtered through Celite. Removal of the solvent under vacuum gave an orange residue. To further purify the product, the residue was extracted with 4 x 5 mL pentane and filtered through Celite. The combined filtrates were evaporated to give 14.7 mg orange powder (76% yield). ^1H and $^{31}P\{^1H\}$ NMR spectra were identical to those of **1**. ^{15}N NMR (51 MHz, C_6D_6): δ 371 (s). FTIR (solid): matches **1** except for new bands at 1036 and 1074 cm^{-1} (see Fig. S15).

*[($P^{O}NP$)Re(N)(Cl)][mCBA] (**2**):* In separate 20 mL vials, 105.6 mg **1** (1.77 x 10^{-4} mol, 1.0 equiv) was suspended in 5 mL Et_2O to form an orange slurry, and 45.8 mg *m*-chloroperbenzoic acid (2.65 x 10^{-4} mol, 1.5 equiv) was dissolved in 3 mL Et_2O to give a colorless solution. The perbenzoic acid solution was quantitatively added to **1** dropwise via pipette while stirring at ambient temperature, resulting in a color change to a gold solution. The reaction was stirred at ambient temperature for 1 hour, after which the reaction was filtered through Celite to remove a brown precipitate. The gold filtrate was concentrated under vacuum to give a sticky yellow solid. This solid was triturated and washed with 4 x 3 mL pentane, then dried under vacuum to yield 114.5 mg **2** as a yellow powder (84% yield), which was pure by ^{1}H and $^{31}P\{^{1}H\}$ NMR spectroscopy. Crystals suitable for X-ray diffraction were grown from a concentrated solution of **2** in Et_2O at –40 °C. ^{1}H NMR (400 MHz, THF-d_8): δ 12.03 (br. s, 1H, O*H*), δ 7.98 (s, 1H, *o-H* of mCBA), δ 7.92 (d, *J* = 7.7 Hz, 1H, *o-H* of mCBA), 7.56 (d, *J* = 8.0 Hz, 1H, *p-H* of mCBA), 7.43 (t, *J* = 7.9 Hz, 1H, *m-H* of mCBA), δ 3.39 (m, 2H, $N(CH_2CH_2)_2$), δ 3.32 (superimposed m, 2H, $N(CH_2CH_2)_2$), δ 2.07 (m, 2H, $N(CH_2CH_2)_2$), δ 1.58 (superimposed m, 2H, $N(CH_2CH_2)_2$), δ 1.54 (vt, 18H, P(*tBu*)(tBu')), δ 1.34 (vt, 18H, P(tBu)(*tBu'*)). $^{13}C\{^{1}H\}$ NMR (126 MHz, THF-d_8) δ 165.55, 133.95, 133.20, 132.18, 129.67, 129.31, 127.74, 66.37, 36.85, 34.64, 28.32, 24.29, 18.99. $^{31}P\{^{1}H\}$ NMR (162 MHz, THF-d_8): δ 64.60 (s). UV-vis (CH_2Cl_2 solution): λ = 332 nm (ε = 1300 $M^{-1}\,cm^{-1}$), 393 nm (shoulder, ε = 290 $M^{-1}\,cm^{-1}$), 458 nm (shoulder, ε = 160 $M^{-1}\,cm^{-1}$). FTIR (solid, cm^{-1}): 3073 (w), 2997, 2981, 2954, 2922, 2899, 2868, 1731 (br), 1607, 1574, 1470, 1429, 1394, 1367, 1278, 1263, 1248, 1210, 1179, 1136, 1077 (s), 1061, 1026, 990, 939, 911, 846 (s), 808 (s), 750 (s), 710 (s), 698, 675, 651, 616, 592 (w), 572 (w), 529, 484, 427. Anal. calcd.(found) for $C_{27}H_{49}Cl_2N_2O_3P_2Re$ (%): C, 42.18(43.04); H, 6.42(6.43); N, 3.64(3.33). We were unable to obtain elemental analysis with closer agreement in carbon.

*[($P^{O}NP$)Re(^{15}N)(Cl)][mCBA] (**2-^{15}N**):* The synthesis of **2-^{15}N** was completed analogously to the synthesis of **2** using **1-^{15}N** as the starting material. ^{1}H and ^{31}P{^{1}H} NMR spectra were identical to those of **2**. ^{15}N NMR (51 MHz, C_6D_6): δ 393 (s). FTIR (solid, cm^{-1}): matches **2** except for a new band at 1042 cm^{-1} (see Fig. S16).

*[($P^{H}NP$)Re(N)(Cl)][OTf] (**3-OTf**):* Compound **3-OTf** was synthesized from **1** according to a literature procedure.[8] ^{1}H and ^{31}P{^{1}H} NMR spectra matched previously reported data. FTIR (solid, cm^{-1}): 3048 (br), 2987, 2967, 2911, 2874, 1480, 1472, 1395, 1371, 1334, 1289 (s), 1241 (s), 1224 (s), 1154 (s), 1108, 1027 (s), 990, 940 (w), 824, 809, 776 (w), 757 (w), 742 (w), 727 (w), 691, 636 (s), 613, 575, 539 (w), 517, 497, 435, 426.

*[($P^{H}NP$)Re(^{15}N)(Cl)][OTf] (**3-^{15}N**):* The synthesis of **3-^{15}N** was completed analogously to the synthesis of **3** using **1-^{15}N** as the starting material. ^{1}H and ^{31}P{^{1}H} NMR spectra were identical to those of **3**. ^{15}N NMR (51 MHz, C_6D_6): δ 387 (s). FTIR (solid, cm^{-1}): matches **3** except for new bands at 1037 and 1074 cm^{-1} (see Fig. S17).

Tris(4-bromo-phenyl)aminium hexafluorophosphate: This compound was synthesized according to a modified literature procedure,[65] in which 1.00 g tris(4-bromo-phenyl)amine (2.08 x 10^{-3} mol, 1.06 equiv) was dissolved in 8 mL CH_2Cl_2 and added via pipette to a slurry of 345 mg [NO][PF_6] (1.97 x 10^{-3} mol, 1 equiv) in 30 mL CH_2Cl_2 at –78 °C while stirring vigorously. Addition of the amine solution was accompanied by a distinct color change to deep blue. The reaction was stirred at –78 °C for 1 h, then allowed to warm to ambient temperature. Removal of the solvent under vacuum gave a dark indigo solid. This residue was slurried in 15 mL Et_2O and filtered. The solid was washed with 2 x 10 mL Et_2O and dried under vacuum for 30 min, resulting in 1.11 g of the compound as an indigo-purple solid (89% yield).

*[(P^{O}NP)Re(N)(Cl)][PF$_6$] (**4**):* In separate vials, 29.9 mg **2** (3.89 x 10^{-5} mol, 1.0 equiv) was dissolved in 3 mL CH_2Cl_2 to give a yellow solution, and 23.0 mg tris(4-bromo-phenyl)aminium hexafluorophosphate (3.67 x 10^{-5} mol, 0.94 equiv) was dissolved in 5 mL CH_2Cl_2 to give a dark blue solution. Both solutions were cooled to –78 °C, and the [Re] solution was added to the aminium dropwise via pipette while stirring. The reaction was stirred at –78 °C for 1 h, after which it had become bright green. The reaction was allowed to warm to ambient temperature, and the solvent was removed under vacuum to give a bright green residue. The product was washed with 4 x 5 mL Et_2O, re-dissolved in 4 mL DCM, layered with 12 mL Et_2O, and left at –40 °C overnight. Decanting the mother liquor and evaporating residual solvent under vacuum gave 25.0 mg **4** as green feathery crystals (85% yield). The ^{1}H NMR spectrum of **4** demonstrates several broad paramagnetic resonances (Fig. S2). ^{1}H NMR (500 MHz, CD_2Cl_2): δ 34.00 (2H, C*H*$_2$), δ 12.12 (18H, P(*tBu*)(tBu')), δ 5.58 (20H, superimposed C*H*$_2$ and P(tBu)(*tBu'*)). UV-vis (CH_2Cl_2 solution): λ = 307 nm (ε = 5000 M^{-1} cm^{-1}), 350 nm (shoulder, ε = 2800 M^{-1} cm^{-1}), 417 nm (shoulder, ε = 580 M^{-1} cm^{-1}), 668 nm (ε = 390 M^{-1} cm^{-1}). FTIR (solid, cm^{-1}): 2971, 2939, 2907, 2873, 1478, 1468, 1445 (w), 1397, 1374, 1245 (w), 1209 (w), 1175, 1058, 1023, 992 (w), 936 (w), 874, 832 (s), 740, 709, 612 (w), 589 (w), 557, 485, 424. Anal. calcd.(found) for $C_{20}H_{44}ClF_6N_2OP_3Re$ (%): C, 31.73(31.75); H, 5.86(5.86); N, 3.70(3.65).

*[(P^{O}NP)Re(^{15}N)(Cl)][PF$_6$] (**4**-^{15}**N**):* Synthesis of **4**-^{15}**N** was completed analogously to the synthesis of **4** using **2**-^{15}**N** as the starting material. FTIR (solid, cm^{-1}): matches **4** except for a new band at 1024 cm^{-1} (see Fig. S18).

*[(PNP)Re(N)(Cl)][PF$_6$] (**5**):* In a 20 mL vial, 30.0 mg **1** (5.03 x 10^{-5} mol, 1.0 equiv) was dissolved in 5 mL CH_2Cl_2 to give an orange solution. The solution was cooled to –78 °C, at which point 15.8 mg [Cp_2Fe][PF_6] (4.78 x 10^{-5} mol, 0.95 equiv) was slowly added as a solid while

stirring. The solution darkened from orange to bright red. The solvent was removed under vacuum while the solution warmed to ambient temperature. The resulting residue was washed with 3 x 5 mL cold (–40 °C) Et_2O to remove Cp_2Fe and residual **1**, leaving behind a pink-red solid. The pink-red solid was dissolved in 3 mL cold (–40 °C) CH_2Cl_2 to give a red solution, which was layered with 10 mL cold (–40 °C) Et_2O and placed in a –40 °C freezer overnight. Decanting the mother liquor and evaporating residual solvent under vacuum gave 28.3 mg pink crystals suitable for X-ray diffraction. ^{1}H NMR spectroscopy of the pink crystals showed that **5** was isolated with 26% **3-PF$_6$** as an impurity, giving an overall yield of 56% for **5**. The ^{1}H NMR spectrum of **5** demonstrates several broad paramagnetic resonances (Fig. S3). ^{1}H NMR (500 MHz, CD_2Cl_2): δ 6.91 (18H, P(*tBu*)(tBu')), δ 4.39 (18H, P(tBu)(*tBu'*)), δ 4.33 (2H, superimposed C*H*$_2$), δ –0.52 (2H, C*H*$_2$). UV-vis (CH_2Cl_2 solution with impurity of **3-PF$_6$**): λ = 291 nm (shoulder, ε = 2500 M^{-1} cm^{-1}), 325 nm (shoulder, ε = 1700 M^{-1} cm^{-1}), 516 nm (ε = 290 M^{-1} cm^{-1}), 627 nm (ε = 90 M^{-1} cm^{-1}). FTIR (solid with impurity of **3-PF$_6$**, cm^{-1}): 3208 (w), 2987, 2969, 2908, 2874, 1480, 1471, 1397, 1372, 1327, 1290 (w), 1281 (w), 1218, 1178, 1109 (w), 1076, 1052, 1021, 988 (w), 968 (w), 943 (w), 832 (s), 782 (s), 740, 716, 693, 611, 583 (w), 557 (s), 519, 479 (s), 443, 422. Anal. calcd.(found) for $C_{20}H_{44}ClF_6N_2P_3Re$ (%): C, 32.41(33.19); H, 5.98(5.99); N, 3.78(3.61). We were unable to obtain elemental analysis with closer agreement in carbon.

*[(PNP)Re(^{15}N)(Cl)][PF$_6$] (**5-^{15}N**):* Synthesis of **5-^{15}N** was completed analogously to synthesis of **5** using **1-^{15}N** as the starting material. FTIR (solid, cm^{-1}): matches **5** except for a new band at 1035 cm^{-1} (see Fig. S19).

Instrumentation and methods. NMR spectra were acquired on an Agilent 400 MHz or 500 MHz spectrometer. ^{1}H spectra were referenced to residual ^{1}H signals from the deuterated solvent with which the sample was prepared,[66] and ^{13}C{^{1}H}, ^{31}P{^{1}H}, and ^{15}N spectra were absolute

referenced to the corresponding ^{1}H spectra. Line fitting of paramagnetic resonances in ^{1}H NMR spectra was done using MestReNova 10.0.1. IR spectra were obtained using a Bruker Alpha spectrometer containing a diamond ATR unit with 2 cm^{-1} resolution.

Electrochemical measurements were collected using a CH Instruments 600D potentiostat in a N_2 glovebox or in solutions purged with dry N_2 gas. Cyclic voltammetry (CV) experiments were conducted in 0.1 M tetrabutylammonium hexafluorophosphate (TBA-PF_6) solutions in dry solvent using a glassy carbon disc working electrode (3.0 mm diameter), a platinum wire auxiliary electrode, and a silver wire psuedoreference. Wire electrodes were sanded and rinsed with dry solvent prior to use, and glassy carbon disc electrodes were polished using 0.05 μm alumina powder and rinsed with dry solvent prior to use. Measurements conducted in THF or CH_2Cl_2 were compensated for internal resistance prior to collecting data. CV experiments were referenced to ferrocene (Cp_2Fe) as an internal standard after completion.

Elemental analyses were obtained from the CENTC Elemental Analysis Facility at the University of Rochester. Microanalysis samples were weighed on a PerkinElmer Model AD-6 Autobalance, analyzed on a PerkinElmer 2400 Series II Analyzer, and handled in a VAC Atmospheres argon glovebox.

Differential EPR spectra were measured on a Bruker EXELSYS E500 spectrometer utilizing a super-high Q resonator and an Oxford ESR-900 helium-flow cryostat at 8–11 K. Instrument parameters: microwave frequency: 9.37 GHz; microwave power: 10 mW; modulation frequency 100 kHz; modulation amplitude: 19.49 G; conversion time: 5.12 ms; time constant: 1.28–2.56 ms. Samples of approximately 0.2 mM were dissolved in glassing solvent mixtures of 1:1 CH_2Cl_2:toluene. Simulations were performed using the 'pepper' function in EasySpin version

5.0.5. Line broadening was simulated using gStrain and Astrain to account for Gaussian distributions in *g* principal values and corresponding *A* values.

ASSOCIATED CONTENT

Supporting Information. The Supporting Information is available free of charge:

Analytical data and spectra for novel complexes, electrochemical data, IR spectra, NMR spectra of reactions, crystallographic data for **1**–**5**, DFT methods, DFT-optimized structures, orbital decomposition, NBO, and SOPT analysis.

AUTHOR INFORMATION

Corresponding Author

*Email: patrick.holland@yale.edu; james.mayer@yale.edu

ACKNOWLEDGMENT

The authors thank Professors Sven Schneider, Alex Miller, and Alan Goldman and their research groups for support and valuable discussions. G.P.C. gratefully acknowledges H. Lant and S. Lee for assistance with EPR experiments, as well as S. Kolmar, A. Speelman, D. Kim, and J. Agarwal for assistance with DFT studies. This work was funded by the U.S. National Science Foundation

(CHE-1665135, with initial support from CHE-1205189 *via* the Center for Enabling New Technologies through Catalysis).

REFERENCES

1. Klopsch, I.; Yuzik-Klimova, E. Y.; Schneider, S., Functionalization of N_2 by Mid to Late Transition Metals via N–N Bond Cleavage. In *Nitrogen Fixation*, Nishibayashi, Y., Ed. Springer International Publishing: Cham, 2017; pp 71-112.
2. Laplaza, C. E.; Cummins, C. C. Dinitrogen Cleavage by a Three-Coordinate Molybdenum(III) Complex. *Science* **1995,** *268*, 861.
3. Laplaza, C. E.; Johnson, M. J. A.; Peters, J.; Odom, A. L.; Kim, E.; Cummins, C. C.; George, G. N.; Pickering, I. J. Dinitrogen Cleavage by Three-Coordinate Molybdenum(III) Complexes: Mechanistic and Structural Data. *J. Am. Chem. Soc.* **1996,** *118*, 8623-8638.
4. Bezdek, M. J.; Chirik, P. J. Expanding Boundaries: N_2 Cleavage and Functionalization beyond Early Transition Metals. *Angew. Chem., Int. Ed.* **2016,** *55*, 7892-7896.
5. Hebden, T. J.; Schrock, R. R.; Takase, M. K.; Mueller, P. Cleavage of Dinitrogen to Yield a (t-BuPOCOP)molybdenum(IV) Nitride. *Chem. Commun.* **2012,** *48*, 1851-1853.
6. Silantyev, G. A.; Foerster, M.; Schluschass, B.; Abbenseth, J.; Wuertele, C.; Volkmann, C.; Holthausen, M. C.; Schneider, S. Dinitrogen Splitting Coupled to Protonation. *Angew. Chem., Int. Ed.* **2017,** *56*, 5872-5876.
7. Ishida, Y.; Kawaguchi, H. Nitrogen Atom Transfer from a Dinitrogen-derived Vanadium Nitride Complex to Carbon Monoxide and Isocyanide. *J. Am. Chem. Soc.* **2014,** *136*, 16990-3.

8. Klopsch, I.; Finger, M.; Wuertele, C.; Milde, B.; Werz, D. B.; Schneider, S. Dinitrogen Splitting and Functionalization in the Coordination Sphere of Rhenium. *J. Am. Chem. Soc.* **2014,** *136*, 6881-6883.

9. Liao, Q.; Cavaille, A.; Saffon-Merceron, N.; Mezailles, N. Direct Synthesis of Silylamine from N_2 and a Silane: Mediated by a Tridentate Phosphine Molybdenum Fragment. *Angew. Chem., Int. Ed.* **2016,** *55*, 11212-11216.

10. Arashiba, K.; Eizawa, A.; Tanaka, H.; Nakajima, K.; Yoshizawa, K.; Nishibayashi, Y. Catalytic Nitrogen Fixation via Direct Cleavage of Nitrogen–Nitrogen Triple Bond of Molecular Dinitrogen under Ambient Reaction Conditions. *Bull. Chem. Soc. Jpn.* **2017,** *90*, 1111-1118.

11. Lindley, B. M.; van Alten, R. S.; Finger, M.; Schendzielorz, F.; Würtele, C.; Miller, A. J. M.; Siewert, I.; Schneider, S. Mechanism of Chemical and Electrochemical N_2 Splitting by a Rhenium Pincer Complex. *J. Am. Chem. Soc.* **2018,** *140*, 7922-7935.

12. Rodriguez, M. M.; Bill, E.; Brennessel, W. W.; Holland, P. L. Reduction and Hydrogenation to Ammonia by a Molecular Iron-Potassium Complex. *Science* **2011,** *334*, 780-783.

13. Miyazaki, T.; Tanaka, H.; Tanabe, Y.; Yuki, M.; Nakajima, K.; Yoshizawa, K.; Nishibayashi, Y. Cleavage and Formation of Molecular Dinitrogen in a Single System Assisted by Molybdenum Complexes Bearing Ferrocenyldiphosphine. *Angew. Chem., Int. Ed.* **2014,** *53*, 11488-11492.

14. MacLeod, K. C.; McWilliams, S. F.; Mercado, B. Q.; Holland, P. L. Stepwise N–H Bond Formation from N_2-derived Iron Nitride, Imide and Amide Intermediates to Ammonia. *Chem. Sci.* **2016,** *7*, 5736-5746.

15. Lee, Y.; Sloane, F. T.; Blondin, G.; Abboud, K. A.; García-Serres, R.; Murray, L. J. Dinitrogen Activation Upon Reduction of a Triiron(II) Complex. *Angew. Chem., Int. Ed.* **2014,** *54*, 1499-1503.

16. Nikiforov, G. B.; Vidyaratne, I.; Gambarotta, S.; Korobkov, I. Titanium-Promoted Dinitrogen Cleavage, Partial Hydrogenation, and Silylation. *Angew. Chem., Int. Ed.* **2009,** *48*, 7415-7419.

17. Akagi, F.; Matsuo, T.; Kawaguchi, H. Dinitrogen Cleavage by a Diniobium Tetrahydride Complex: Formation of a Nitride and Its Conversion into Imide Species. *Angew. Chem., Int. Ed.* **2007,** *46*, 8778-8781.

18. Shima, T.; Hu, S.; Luo, G.; Kang, X.; Luo, Y.; Hou, Z. Dinitrogen Cleavage and Hydrogenation by a Trinuclear Titanium Polyhydride Complex. *Science* **2013,** *340*, 1549.

19. Curley, J. J.; Sceats, E. L.; Cummins, C. C. A Cycle for Organic Nitrile Synthesis via Dinitrogen Cleavage. *J. Am. Chem. Soc.* **2006,** *128*, 14036-14037.

20. Guru, M. M.; Shima, T.; Hou, Z. Conversion of Dinitrogen to Nitriles at a Multinuclear Titanium Framework. *Angew. Chem., Int. Ed.* **2016,** *55*, 12316-12320.

21. Klopsch, I.; Kinauer, M.; Finger, M.; Wurtele, C.; Schneider, S. Conversion of Dinitrogen into Acetonitrile under Ambient Conditions. *Angew. Chem., Int. Ed.* **2016,** *55*, 4786-9.

22. Man, W.-L.; Lam, W. W. Y.; Lau, T.-C. Reactivity of Nitrido Complexes of Ruthenium(VI), Osmium(VI), and Manganese(V) Bearing Schiff Base and Simple Anionic Ligands. *Acc. Chem. Res.* **2014,** *47*, 427-439.

23. Berry, J. F. Terminal Nitrido and Imido Complexes of the Late Transition Metals. *Comments Inorg. Chem.* **2009,** *30*, 28-66.

24. Smith, J. M. Reactive Transition Metal Nitride Complexes. *Prog. Inorg. Chem.* **2014,** *58*, 417-470.

25. Schendzielorz, F. S.; Finger, M.; Volkmann, C.; Wurtele, C.; Schneider, S. A Terminal Osmium(IV) Nitride: Ammonia Formation and Ambiphilic Reactivity. *Angew. Chem., Int. Ed.* **2016,** *55*, 11417-20.

26. Williams, D. S.; Meyer, T. J.; White, P. S. Preparation of Osmium(II) Nitrosyls by Direct Oxidation of Osmium(VI) Nitrides. *J. Am. Chem. Soc.* **1995,** *117*, 823-4.

27. Coia, G. M.; Demadis, K. D.; Meyer, T. J. Oxidation of Ammonia in Osmium Polypyridyl Complexes. *Inorg. Chem.* **2000,** *39*, 2212-2223.

28. Crevier, T. J.; Lovell, S.; Mayer, J. M.; Rheingold, A. L.; Guzei, I. A. Chalcogen Atom Transfer to a Metal Nitrido. The First Transition Metal Selenonitrosyl Complex. *J. Am. Chem. Soc.* **1998,** *120*, 6607-6608.

29. Walstrom, A.; Pink, M.; Fan, H.; Tomaszewski, J.; Caulton, K. G. Radical (NO) and Nonradical (N_2O) Reagents Convert a Ruthenium(IV) Nitride to the Same Nitrosyl Complex. *Inorg. Chem.* **2007,** *46*, 7704-7706.

30. Scheibel, M. G.; Askevold, B.; Heinemann, F. W.; Reijerse, E. J.; de Bruin, B.; Schneider, S. Closed-shell and Open-shell Square-planar Iridium Nitrido Complexes. *Nat. Chem.* **2012,** *4*, 552-558.

31. Clarkson, S. G.; Basolo, F. Reaction of Some Cobalt Nitrosyl Complexes with Oxygen. *Inorg. Chem.* **1973,** *12*, 1528-34.

32. Ugo, R.; Bhaduri, S.; Johnson, B. F. G.; Khair, A.; Pickard, A.; Benn-Taarit, Y. Oxygenation of the Nitrosyl Ligand in Complexes of Nickel and Platinum. *J. Chem. Soc., Chem. Commun.* **1976**, 694-5.

33. Tovrog, B. S.; Diamond, S. E.; Mares, F. Oxygen Transfer from Ligands: Cobalt Nitro Complexes as Oxygenation Catalysts. *J. Am. Chem. Soc.* **1979,** *101*, 270-2.

34. Pipes, D. W.; Meyer, T. J. Comparisons Between Polypyridyl Nitrosyl Complexes of Osmium(II) and Ruthenium(II). *Inorg. Chem.* **1984,** *23*, 2466-72.

35. Fernandez, B. O.; Lorkovic, I. M.; Ford, P. C. Mechanisms of Ferriheme Reduction by Nitric Oxide: Nitrite and General Base Catalysis. *Inorg. Chem.* **2004,** *43*, 5393-5402.

36. Zhang, J.-Y.; Liu, C.-M.; Zhang, D.-Q.; Gao, S.; Zhu, D.-B. Syntheses, Crystal Structures, and Magnetic Properties of two Cyclic Dimer M_2L_2 Complexes Constructed from a New Nitronyl Nitroxide Ligand and $M(hfac)_2$ ($M = Cu^{2+}$, Mn^{2+}). *Inorg. Chim. Acta* **2007,** *360*, 3553-3559.

37. Okamura, Y.; Ishii, N.; Nogami, T.; Ishida, T. Hard Magnets after Freezing of Spin Dynamics of Soft Magnets in Cobalt(II)-radical Chain Compounds. *Bull. Chem. Soc. Jpn.* **2010,** *83*, 716-725.

38. Boreen, M. A.; Bogart, J. A.; Carroll, P. J.; Schelter, E. J. Rearrangement in a Tripodal Nitroxide Ligand To Modulate the Reactivity of a Ti-F Bond. *Inorg. Chem.* **2015,** *54*, 9588-9593.

39. Chen, S.-J.; Zhang, X.-H.; Yu, X.; Qiu, H.; Yap, G. P. A.; Guzei, I. A.; Lin, Z.; Wu, Y.-D.; Xue, Z.-L. Reaction of $Ta(NMe_2)_5$ with O_2: Formation of Aminooxy and

Unusual (Aminomethyl)amide Oxo Complexes and Theoretical Studies of the Mechanistic Pathways. *J. Am. Chem. Soc.* **2007,** *129*, 14408-14421.

40. Graham, T. W.; Tsang, C.-W.; Chen, X.; Guo, R.; Jia, W.; Lu, S.-M.; Sui-Seng, C.; Ewart, C. B.; Lough, A.; Amoroso, D.; Abdur-Rashid, K. Catalytic Solvolysis of Ammonia Borane. *Angew. Chem., Int. Ed.* **2010,** *49*, 8708-8711.

41. Nielsen, M.; Kammer, A.; Cozzula, D.; Junge, H.; Gladiali, S.; Beller, M. Efficient Hydrogen Production from Alcohols under Mild Reaction Conditions. *Angew. Chem., Int. Ed.* **2011,** *50*, 9593-9597.

42. Han, Z.; Rong, L.; Wu, J.; Zhang, L.; Wang, Z.; Ding, K. Catalytic Hydrogenation of Cyclic Carbonates: A Practical Approach from CO_2 and Epoxides to Methanol and Diols. *Angew. Chem., Int. Ed.* **2012,** *51*, 13041-13045.

43. Choi, J.-H.; Prechtl, M. H. G. Tuneable Hydrogenation of Nitriles into Imines or Amines with a Ruthenium Pincer Complex under Mild Conditions. *ChemCatChem* **2015,** *7*, 1023-1028.

44. Schiwek, C.; Meiners, J.; Foerster, M.; Wuertele, C.; Diefenbach, M.; Holthausen, M. C.; Schneider, S. Oxygen Reduction with a Bifunctional Iridium Dihydride Complex. *Angew. Chem., Int. Ed.* **2015,** *54*, 15271-15275.

45. Fu, S.; Chen, N.-Y.; Liu, X.; Shao, Z.; Luo, S.-P.; Liu, Q. Ligand-Controlled Cobalt-Catalyzed Transfer Hydrogenation of Alkynes: Stereodivergent Synthesis of Z- and E-Alkenes. *J. Am. Chem. Soc.* **2016,** *138*, 8588-8594.

46. Fu, S.; Shao, Z.; Wang, Y.; Liu, Q. Manganese-Catalyzed Upgrading of Ethanol into 1-Butanol. *J. Am. Chem. Soc.* **2017,** *139*, 11941-11948.

47. Affan, M. A.; Jessop, P. G. Catalytic Formylation of Primary and Secondary Amines with CO_2 and H_2 Using Abundant-Metal Catalysts. *Inorg. Chem.* **2017,** *56*, 7301-7305.

48. Nguyen, D. H.; Trivelli, X.; Capet, F.; Paul, J.-F.; Dumeignil, F.; Gauvin, R. M. Manganese Pincer Complexes for the Base-Free, Acceptorless Dehydrogenative Coupling of Alcohols to Esters: Development, Scope, and Understanding. *ACS Catal.* **2017,** *7*, 2022-2032.

49. Wiberg, K. B. Application of the Pople-Santry-Segal CNDO Method to the Cyclopropylcarbinyl and Cyclobutyl Cation and to Bicyclobutane. *Tetrahedron* **1968,** *24*, 1083-1096.

50. Reed, A. E.; Curtiss, L. A.; Weinhold, F. Intermolecular Interactions from a Natural Bond Orbital, Donor-acceptor Viewpoint. *Chem. Rev.* **1988,** *88*, 899-926.

51. Voigt, A.; Abram, U.; Kirmse, R. The Existence of $[ReNF_4]^-$ – An EPR Study. *Inorg. Chem. Commun.* **1998,** *1*, 141-142.

52. Voigt, A.; Abram, U.; Strauch, P.; Kirmse, R. An Electron Paramagnetic Resonance Study of Tetra-n-butylammonium Tetrabromonitridorhenate(VI), $[(n\text{-}C_4H_9)_4N][ReNBr_4]$. *Inorg. Chim. Acta* **1998,** *271*, 199-202.

53. Abram, U.; Braun, M.; Abram, S.; Kirmse, R.; Voigt, A. [NBu4][ReNCl4]: Facile Synthesis, Structure, Electron Paramagnetic Resonance Spectroscopy and Reactions. *J. Chem. Soc., Dalton Trans.* **1998**, 231-238.

54. Badger, R. M. Relation Between the Internuclear Distances and Force Constants of Molecules and Its Application to Polyatomic Molecules. *J. Chem. Phys.* **1935,** *3*, 710-14.

55. Laihia, K.; Kolehmainen, E.; Kauppinen, R.; Lorenc, J.; Puszko, A. Multinuclear ^{1}H, ^{13}C and ^{15}N NMR Study of Some Substituted 2-amino-4-nitropyridines and Their N-oxides. *Spectrochim. Acta, Part A* **2002,** *58A*, 1425-1435.

56. Wrackmeyer, B. Calculation of ^{15}N NMR Parameters of Azides and Some Related Compounds. Revisiting the Methylation of Nitrous Oxide N_2O. *Z. Naturforsch., B: J. Chem. Sci.* **2011,** *66*, 1079-1082.

57. Perinu, C.; Saramakoon, G.; Arstad, B.; Jens, K.-J. Application of ^{15}N-NMR Spectroscopy to Analysis of Amine Based CO_2 Capture Solvents. *Energy Procedia* **2014,** *63*, 1144-1150.

58. Galajov, M.; Garcia, C.; Gomez, M. Tri-chlorido, 2-methylallyl and 2-butenyl Tert-butylimido Niobium and Tantalum Complexes: Synthesis, Multinuclear NMR Spectroscopy and Reactivity. *Dalton Trans.* **2011,** *40*, 413-420.

59. Galajov, M.; Garcia, C.; Gomez, M.; Gomez-Sal, P.; Temprado, M. Synthesis and DFT, Multinuclear Magnetic Resonance, and X-ray Structural Studies of Iminoacyl Imido Hydridotris(3,5-dimethylpyrazolyl)borate Niobium and Tantalum(V) Complexes. *Organometallics* **2014,** *33*, 2277-2286.

60. Scepaniak, J. J.; Margarit, C. G.; Harvey, J. N.; Smith, J. M. Nitrogen Atom Transfer from Iron(IV) Nitrido Complexes: A Dual-Nature Transition State for Atom Transfer. *Inorg. Chem.* **2011,** *50*, 9508-9517.

61. Johnson, N. P.; Lock, C. J. L.; Wilkinson, G. Amine, Phosphine, Arsine, and Stilbine Complexes of Rhenium(III), -(IV), and -(V). *J. Chem. Soc.* **1964**, 1054-66.

62. Rouschias, G.; Wilkinson, G. Preparation and Reactions of Trihalo(alkanonitrile)bis(triphenylphosphine) Rhenium(III) Complexes. *J. Chem. Soc. A* **1967**, 993-1000.

63. Schulz, A.; Villinger, A. Binary Polyazides of Cadmium and Mercury. *Chem. - Eur. J.* **2015,** *21*, 3649-3663.

64. Demadis, K. D.; Meyer, T. J.; White, P. S. Reactivity of Osmium(VI) Nitrides with the Azide Ion. A New Synthetic Route to Osmium(II) Polypyridyl Complexes. *Inorg. Chem.* **1998,** *37*, 3610-3619.

65. Rhile, I. J.; Markle, T. F.; Nagao, H.; DiPasquale, A. G.; Lam, O. P.; Lockwood, M. A.; Rotter, K.; Mayer, J. M. Concerted Proton−Electron Transfer in the Oxidation of Hydrogen-Bonded Phenols. *J. Am. Chem. Soc.* **2006,** *128*, 6075-6088.

66. Fulmer, G. R.; Miller, A. J. M.; Sherden, N. H.; Gottlieb, H. E.; Nudelman, A.; Stoltz, B. M.; Bercaw, J. E.; Goldberg, K. I. NMR Chemical Shifts of Trace Impurities: Common Laboratory Solvents, Organics, and Gases in Deuterated Solvents Relevant to the Organometallic Chemist. *Organometallics* **2010,** *29*, 2176-2179.

TABLE OF CONTENTS SYNOPSIS:

The reactivity of an N_2-derived nitride shifts from nucleophilic to electrophilic upon chemical oxidation of the coordinated pincer ligand, forming a novel nitroxide-pincer ligand, and one-electron oxidation of the Re metal center.

TABLE OF CONTENTS GRAPHIC: